Biomaterials 30 (2009) 58–70

Contents lists available at ScienceDirect

Biomaterials

journal homepage: www.elsevier.com/locate/biomaterials

# *In vivo* mineralization and osteogenesis of nanocomposite scaffold of poly (lactide-*co*-glycolide) and hydroxyapatite surface-grafted with poly(L-lactide)

Peibiao Zhang [a], Zhongkui Hong [a], Ting Yu [b], Xuesi Chen [a,*], Xiabin Jing [a]

[a] State Key Laboratory of Polymer Physics and chemistry, Changchun Institute of Applied Chemistry, Chinese Academy of Sciences, Changchun 130022, PR China
[b] School of Public Health, Jilin University, Changchun 130021, PR China

ARTICLE INFO

*Article history:*
Received 2 July 2008
Accepted 28 August 2008
Available online 5 October 2008

*Keywords:*
Poly(lactide-*co*-glycolide)
Hydroxyapatite
Nanocomposite
Mineralization
Osteogenesis
Bone repair

ABSTRACT

Nanocomposite of hydroxyapatite (HAP) surface-grafted with poly(L-lactide) (PLLA) (*g*-HAP) shows a wide application for bone fixation materials due to its improved interface compatibility, mechanical property and biocompatibility in our previous study. In this paper, a 3-D porous scaffold of *g*-HAP/poly (lactide-*co*-glycolide) (PLGA) was fabricated using the solvent casting/particulate leaching method to investigate its applications in bone replacement and tissue engineering. The composite of un-grafted HAP/PLGA and neat PLGA were used as controls. Their *in vivo* mineralization and osteogenesis were investigated by intramuscular implantation and replacement for repairing radius defects of rabbits. After surface modification, more uniform distribution of *g*-HAP particles but a lower calcium exposure on the surface of *g*-HAP/PLGA was observed. Intramuscular implantation study showed that the scaffold of *g*-HAP/PLGA was more stable than that of PLGA, and exhibited similar mineralization and biodegradability to HAP/PLGA at the 12–20 weeks post-surgery. The implantation study for repairing critical radius defects showed that the scaffold of *g*-HAP/PLGA exhibited rapid and strong mineralization and osteoconductivity, and the incorporation of BMP-2 could enhance the osteogenic process of the composite implant. The new bone formation with the intact structure of a long bone was guided by the implant of *g*-HAP/PLGA.



## 1. Introduction

One of the main goals in bone tissue engineering is to develop biodegradable materials as bone graft substitutes, especially for filling large defects [1–4]. Besides bone forming cells and growth factors, synthetic biomaterials served as scaffolds play a critical role in bone tissue engineering and osteogenesis. They provide a three-dimensional (3-D) space for cell growth and extracellular matrix (ECM) formation, and structural support for the newly formed bone tissue. The ideal synthetic scaffolds for osteogenesis should meet certain criteria to serve this function, including good biocompatibility, sufficient mechanical properties, and adequate biodegradability at a controlled rate commensurate with remodeling [5,6].

Being the major mineral component of natural bone and structurally similar to the bone, hydroxyapatite (HA) is the prospective one of inorganic biomaterials for bone regeneration. HA ceramics were high biocompatible in bone tissue and had a high osteogenic potential (osteoconduction and osteointegration), but the brittleness and fatigue failure in the body limit their clinical applications only for unloading bearing repair and substitute [2,7]. Another outstanding problem of HA ceramics is their bad biodegradability. Sintered HA materials showed no detectable resorption over a period of 9 months of implantation [8].

On the other hand, biodegradable synthetic polyesters, such as poly(lactic acid)(PLA), poly(glycolic acid)(PGA) and their copolymer poly(lactide-*co*-glycolide) (PLGA), have a relatively long history of use in a number of clinical applications [6]. PLGA is one of the most prospective matrices and often used as a construct material for tissue engineering. The mechanical properties and biodegradation rate of PLGA can be manipulated to some extent by controlling the molecular weight of the copolymer and the unit ratio of lactide to glycolide in the copolymer. PLGA copolymers used in bone repair applications have shown to be biocompatible, non-toxic and non-inflammatory [9,10]. However, PLGA cannot be utilized as the load-bearing applications either for its low mechanical strength, too flexible characteristic and lack of osteogenic bioactivity. Thus, the combination of advantages of the two biomaterials will reach some desired properties prior to one of them alone [11].

A series of bioceramic/polymer composites have been developed for bone fixation and bone repairing applications with some attractive properties [12–14]. Especially, nano-HAP is of current

* Corresponding author. State Key Laboratory of Polymer Physics and Chemistry, Changchun Institute of Applied Chemistry, Chinese Academy of Sciences, 5625 Renmin Street, Changchun 130022, PR China. Tel.: +86 43185 262 112; fax: +86 43185 685 653.
*E-mail address:* xschen@ciac.jl.cn (X. Chen).

0142-9612/$ – see front matter © 2008 Elsevier Ltd. All rights reserved.
doi:10.1016/j.biomaterials.2008.08.041

interest because it possesses some special properties, including large specific surface area, improved biodegradability and biological activity. Biodegradable nano-HAP/polymer composites are considered as temporary substitutes of natural bones in that they are both composed of nano-scale HAP and organic compounds (PLGA or collagen). The more synthetic nano-HAP resemble natural bone minerals in composition, size and morphology, the better osteoconductivity would be achieved [15,16]. The introduction of nano-HAP greatly increased the mechanical properties of the nano-hydroxyapatite/polymer composite scaffold and improved the protein adsorption capacity [14]. It has been found that proteins in mineralized tissues act as nature's crystal engineers, where they play a key role in promoting or inhibiting the growth of minerals such as hydroxyapatite [17]. The higher exposure of HA nanoparticles at the scaffold surface may result in significantly higher mineralization and the enhanced bone formation [18].

However, for these nanocomposites, the interface compatibility and binding between nano-HAP filler and a polymer are critical factors to determine the distribution of nano-HA in matrix and mechanical properties of the composite. The lack of adhesion between the two phases will result in an early failure at the interface and, thus, deteriorate the mechanical property and structure stability of scaffold.

In our previous work, nano-hydroxyapatite (HAP) particles surface-grafted with poly(L-lactide) (PLLA) (*g*-HAP) were synthesized and the nanocomposites of *g*-HAP/PLLA (or *g*-HAP/PLGA) showed a wide potential application for bone fixation materials due to its improved interface compatibility, mechanical properties and good biocompatibility [19–21]. To investigate the possible applications of the composites for bone replacement material and tissue engineering scaffold, the nanocomposite of *g*-HAP/PLGA was obtained by mixing 10 wt% *g*-HAP nanoparticles into PLGA matrix. The porous scaffolds of *g*-HAP/PLGA were fabricated with the solvent casting/particulate leaching method. The assessments of their *in vivo* mineralization and osteogenesis were undertaken by intramuscular implantation and replacement for repairing radius defects of rabbits.

## 2. Materials and methods

### 2.1. Preparation of porous scaffold

Poly(lactide-*co*-glycolide) (PLGA, LA/GA = 80:20) we employed was synthesized in our lab [21]. Its viscosity average molecular weight ($M_w$) was about 196,000. The preparation of virgin hydroxyapatite nano-particles (HAP) and their surface-grafting by PLLA (*g*-HAP) have been described in our previous papers [19,21]. Briefly, HAP was synthesized according to the reaction shown in Eq. (1):

$$10\ Ca(OH)_2 + 6\ H_3PO_4 \xrightarrow{60\text{-}80^\circ C} Ca_{10}(PO_4)_6(OH)_2 + 18\ H_2O \quad (1)$$

It was an acicular crystal of about 100 nm in length and 20–40 nm in width, with the atomic ratio Ca/P ≈ 1.67. Then, L-lactide was ring-opening polymerized onto the surface of HAP particles in the presence of stannous octoate (Sn(Oct)) catalyst to afford *g*-HAP according to Eq. (2):

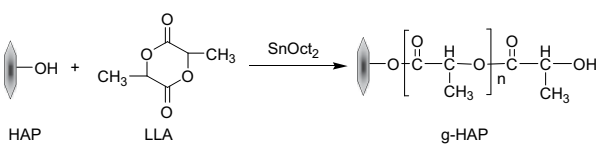


(2)

The amount of grafted polymer on the surface of *g*-HAP was determined by thermal gravimetric analysis to be about 5.0 wt%.

The composites of the *g*-HAP/PLGA and the HAP/PLGA were prepared through *g*-HAP or HAP nano-particle pre-suspended in a certain volume of chloroform and mixed into a 10% PLGA/chloroform solution with the help of magnetic stirring for overnight and ultrasonic treatment for 30 min. The *g*-HAP or HAP content was 10 wt% in the composite.

The sucrose particles with 100–450 μm in diameter obtained with sieves were mixed into the solutions of *g*-HAP/PLGA, HAP/PLGA and PLGA. The mixtures were cast in glass disks and dried in the air for 3 days. The composites (or PLGA)/sucrose mass ratio was 1:6 (w/w). The sucrose particles were subsequently removed from the composites by leaching the composites in distilled water for 5 days with water changed every 12 h and then the composites were dried under air and vacuum. Obtained porous scaffolds of the composites were then cut into small bars (0.3 cm in width, 2.0 cm in length), and sterilized with UV irradiation for 30 min.

**Fig. 1.** Bilateral rabbit radius defects were created by removing 2.0 cm of midshaft diaphyseal bone.

### 2.2. Scaffolds characterization

The porosity values of the scaffolds were measured by liquid displacement according to a published method [22]. Briefly, a sample of weight $W$ was immersed in a graduated cylinder containing a known volume ($V_1$) of ethanol, and a series of brief evacuation–repressurization cycles were conducted to force the ethanol into the pores of the sample. Cycling was continued until no air bubbles were observed emerging from the sample. The total volume of ethanol and the ethanol-impregnated scaffold was then recorded as $V_2$. The ethanol-impregnated sample was removed from the cylinder carefully and the residual ethanol volume was recorded as $V_3$. The volume of the ethanol held in the foam was $V_1 - V_3$, which was determined as the void volume of the foam. The total volume of the foam was $V_2 - V_3$. Thus the open porosity of the sample ($\varepsilon$) was obtained by: $\varepsilon = (V_1 - V_3)/(V_2 - V_3)$.

Meanwhile, samples were cut and coated with Au/Pd in a sputter coater. The pore structure of the porous scaffolds of *g*-HAP/PLGA, HAP/PLGA and PLGA was studied under an emission scanning electron microscope (ESEM) (Philips XL30 ESEM FEG, Japan). 200 pores of each material were measured with NIH Image J. For characterizing the distribution and exposure degrees of *g*-HAP or HAP in PLGA matrix, it was analyzed with energy dispersive X-ray spectrometry (EDX) (Philips, XL-30W/TMP, Japan).

### 2.3. Intramuscular implantation

The cell-free porous scaffolds of *g*-HAP/PLGA, HAP/PLGA and PLGA were implanted intramuscularly for *in vivo* biodegradation and mineralization assessment. The implants of 0.3 cm in width and 2.0 cm in length were embedded into dorsal muscle of 18 rabbits by the surgery. Three parallel samples in a rabbit were used for each material. After surgery, the rabbits were sacrificed with an air injection at 4, 8, 12 and 20 weeks. The implants were taken out and macroscopic observation were undertaken and recorded with a digital camera (Fujifilm FinePix S602, China). The samples were then fixed with 4% paraformaldehyde for 2 h at room temperature. Three samples of each material at every interval time were washed with distilled water three times and freeze-dried for 48 h for SEM, computer radiograph (CR) and calcium content analysis. The other biopsy samples were treated for histological analysis. The analysis processes are briefly described as follows.

### 2.4. Implantation for repairing radius defect

Bilateral critically sized defects of 12 rabbits were created with saw and drill in the radius of each rabbit forelimb by removing 2.0 cm of midshaft diaphyseal bone as shown in Fig. 1. The porous scaffold bars (0.3 cm in width, 2.0 cm in length) of PLGA, HAP/PLGA, *g*-HAP/PLGA and BMP-2/*g*-HAP/PLGA were placed into the defects of different rabbits, respectively. The BMP-2/*g*-HAP/PLGA scaffolds were prepared

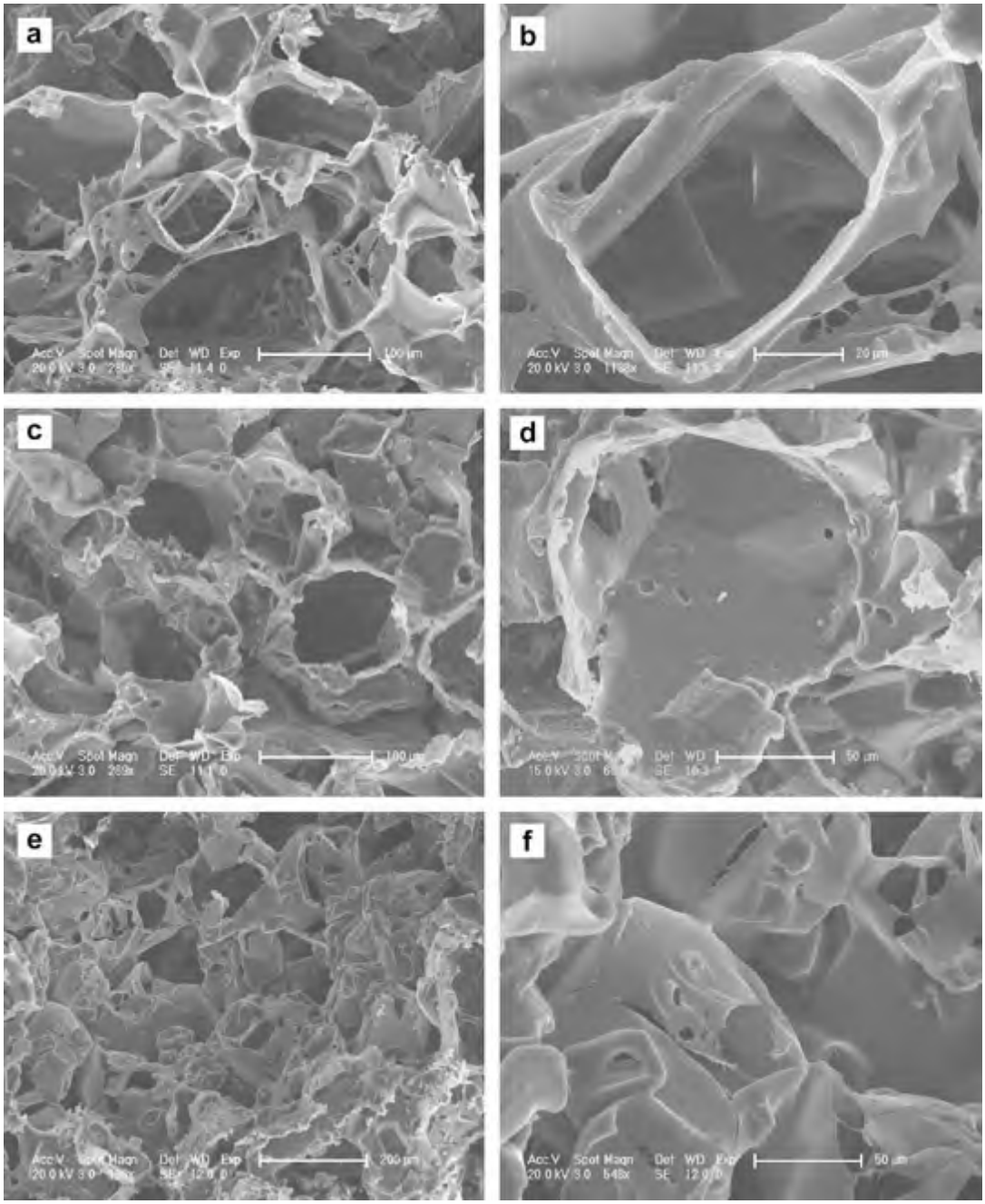


**Fig. 2.** SEM micro-photographs of porous scaffolds of *g*-HAP/PLGA (a and b), HAP/PLGA (c and d) and PLGA (e and f) fabricated with the solvent casting/particulate leaching method. Bar lengths are 200 μm (e), 100 μm (a and c), 50 μm (d and f) and 20 μm (b).

through *g*-HAP/PLGA scaffolds sunk in 100 ng/ml BMP-2 in PBS solution at 4 °C for overnight. The wounds were closed with silk threads in layers. After surgery, the rabbits were returned to their cages and allowed to move freely. All rabbits were injected daily with penicillin intramuscularly in a dose of 200,000 units for each one for 3 days. All the wounds healed gradually and the rabbits were active with no post-surgery complications.

### 2.5. X-ray examination

*In vivo* mineralization and osteogenesis at the rabbit radius defects repaired with PLGA, HAP/PLGA, *g*-HAP/PLGA and BMP-2/*g*-HAP/PLGA were examined with computer radiograph (CR, Kodak CR-400plus, USA) at 0 (the first day after surgery), 2, 4 and 8 weeks post-surgery. The rabbits were exposed to X-ray in prone position as shown in Fig. 1 during anesthetization.

Meanwhile, the *ex vivo* intramuscular implants of *g*-HAP/PLGA, HAP/PLGA and PLGA scaffolds for 4, 8, 12 and 20 weeks post-surgery were examined with CR.

### 2.6. ICP-AES analysis for calcium content measurement

The calcium content of the intramuscular implants of *g*-HAP/PLGA, HAP/PLGA and PLGA for 4, 8, 12 and 20 weeks post-surgery, as well as the scaffolds pre-surgery, was determined using the inductance coupling plasma atom emission spectrum (ICP-AES) (Leeman Prodigy High Dispersion ICP, USA). About 10.0 mg of a sample was taken and quantified precisely before the sample was digested completely with 5.0 ml nitric acid, vaporized, and dissolved in 10.0 ml distilled water. The calcium concentration of the solution was analyzed by ICP-AES. Finally, the calcium content of the implant sample was calculated according to the obtained concentration. Three parallel samples of each material at all time intervals were analyzed.

### 2.7. Histological analysis

Histological analysis of the implants at 8 weeks post-surgery was undertaken. The samples were fixed with 4% paraformaldehyde for 24 h, decalcified in 10% EDTA

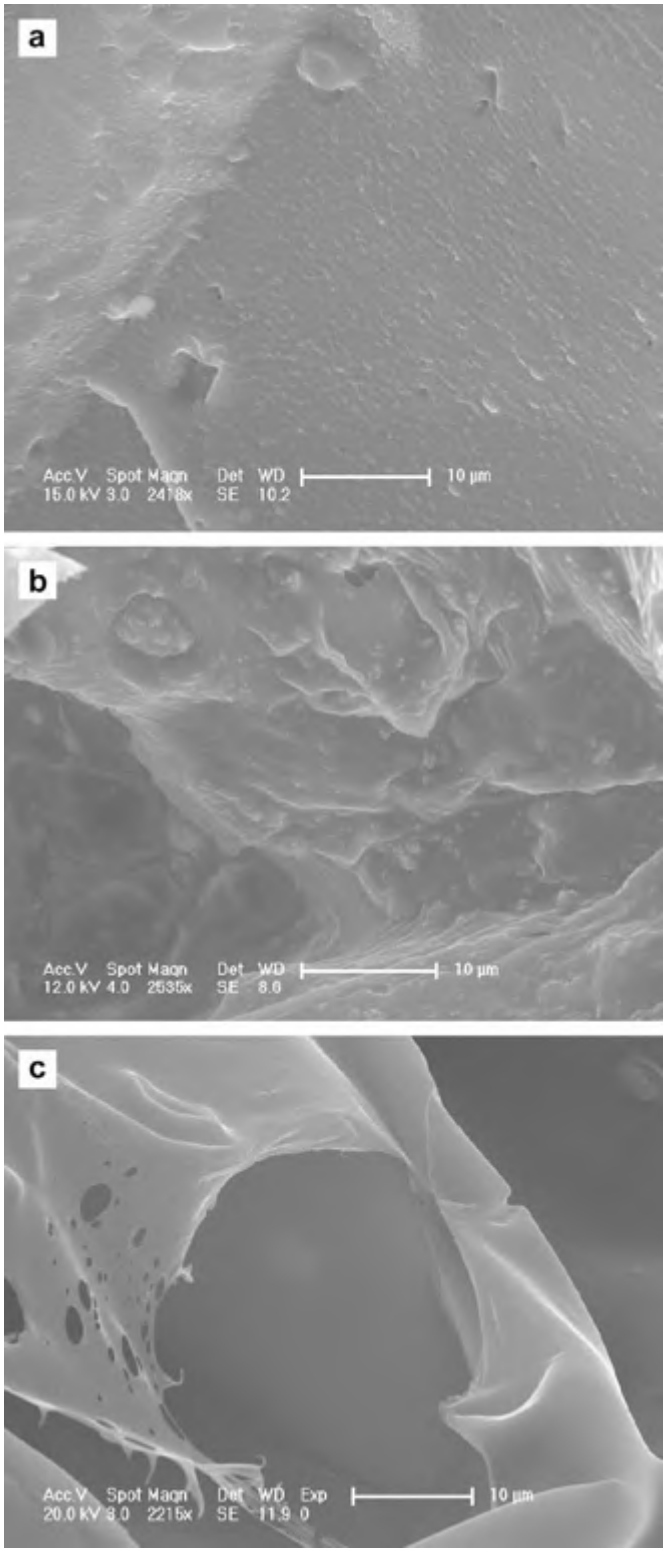


**Fig. 3.** SEM analysis showed the topography of the pore wall surface of *g*-HAP/PLGA (a), HAP/PLGA (b) and PLGA (c) porous scaffold. The different appearances of rough pore wall in composite scaffolds of *g*-HAP/PLGA (a) and HAP/PLGA scaffold (b), and smooth pore wall in pure PLGA scaffold (c) are shown clearly. Moreover, *g*-HAP/PLGA exhibits more uniform granules on the pore wall surface than HAP/PLGA. All bar lengths are 10 μm (a–c).

for 2–4 weeks, embedded in paraffin, and cut using a microtome (Leika RM2145 microtome, Germany) to yield 5 μm thick sections. The sections were stained with haematoxylin and eosin (H&E), and Masson's trichrome staining, and evaluated under light microscopy.

**Table 1**
Pore size (μm) of *g*-HAP/PLGA, HAP/PLGA, PLGA porous scaffolds fabricated with the solvent casting/particulate leaching method

| | Min | Max | Mean | SD |
|---|---|---|---|---|
| *g*-HAP/PLGA | 50.5 | 448.1 | 152.5 | 76.1 |
| HAP/PLGA | 51.6 | 446.0 | 146.9 | 65.4 |
| PLGA | 35.0 | 442.5 | 137.3 | 53.2 |

### 2.8. Statistics analysis

All quantitative data were analyzed with Origin 7.0 (OriginLab Corporation, USA) and expressed as the mean ± standard deviation. Statistical comparisons were carried out using analysis of variance (ANOVA, Origin 7.0). A value of $p < 0.05$ was considered to be statistically significant.

## 3. Results

### 3.1. Scaffold characterization

#### 3.1.1. Scanning electric microscope (SEM) and porosity analysis

The microstructures of the three-dimensional (3-D) porous scaffolds of *g*-HAP/PLGA, HAP/PLGA and PLGA fabricated with the solution casting/particulate leaching method were analyzed with SEM (Figs. 2 and 3). Fig. 2 shows that all scaffolds we fabricated have the irregular macro-pores and the pores are interconnected. The average pore diameters of *g*-HAP/PLGA, HAP/PLGA and PLGA scaffold materials are 148.2 ± 76.1, 146.9 ± 65.4 and 137.3 ± 53.2 μm, respectively (Table 1). The opening porosities of *g*-HAP/PLGA, HAP/PLGA and PLGA scaffolds are 86.6 + 0.9%, 85.9 + 4.6% and 83.6 + 2.4%, respectively. However, there are no significant differences in pore size and opening porosity among the three scaffolds ($P > 0.05$).

Fig. 3 shows the surface topography of the pore wall in scaffolds. The pore wall in the composites of *g*-HAP/PLGA and HAP/PLGA is rough because of 10 wt% nano-*g*-HAP or HAP filled into the PLGA matrix. The distinct difference between *g*-HAP/PLGA and HAP/PLGA is that there is more uniform distribution of granules on the pore wall surface of *g*-HAP/PLGA than that of HAP/PLGA (Fig. 3a and b). The aggregation of un-grafted HAP to a larger particle (about 2–5 μm in diameter) is observed universally in HAP/PLGA scaffold (Fig. 3b). Compared to the nanocomposite scaffolds, the flatter pores (Fig. 2f) and the rather smooth pore wall (Fig. 3c) are shown in pure PLGA scaffold. It indicated that there are more stable microstructures in *g*-HAP/PLGA and HAP/PLGA

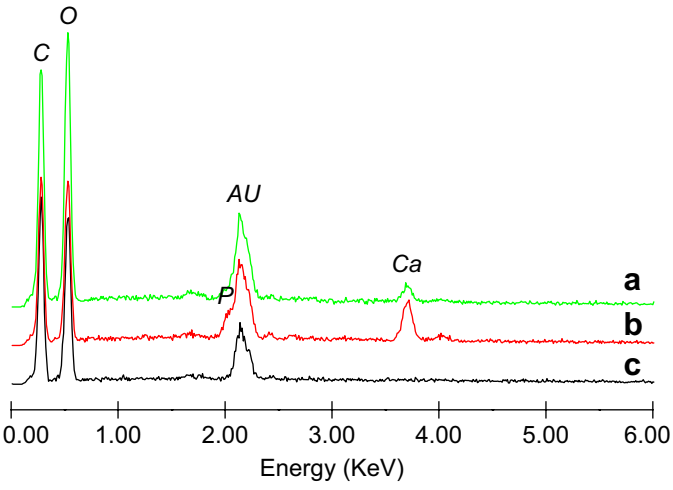


**Fig. 4.** EDX analysis showing the contents of calcium and phosphorus on the surfaces of *g*-HAP/PLGA (a), HAP/PLGA (b) and PLGA (c) porous scaffolds.

nanocomposite scaffolds, and surface modification of HAP grafted with PLLA (*g*-HAP) can improve distribution of the nano-particles on the surface of the composite scaffolds more uniformly than those un-grafted.

*3.1.2. Energy dispersive X-ray spectrometry (EDX) analysis*

EDX element analysis was used to assess the content of calcium (Ca) and phosphor (P) elements on the surface of porous scaffolds. The results showed that the levels of Ca and P exposure on the surface of *g*-HAP/PLGA were lower than that on HAP/PLGA scaffold (Fig. 4). In contrast, there is no calcium and phosphor exposure on the surface of PLGA scaffold. It indicated that the surface modification of HAP particles grafted with poly(L-lactide) will decrease calcium exposure on the composite surface of *g*-HAP/PLGA to a certain extent due to surface-grafted HAP particles covered with a layer of PLLA and embedded in PLGA matrix for its improved interface between HAP and PLGA.

*3.2. Intramuscular implantation*

*3.2.1. Macroscopic observation*

The porous scaffolds of *g*-HAP/PLGA, HAP/PLGA and PLGA embedded in rabbit dorsal muscles were taken out at 4, 8, 12 and 20 weeks post-surgery, and analyzed with macroscopic observation (Fig. 5). At the initial 8 weeks post-surgery, all intramuscular implants of *g*-HAP/PLGA, HAP/PLGA and PLGA kept their original shape. The implants have flesh-colored appearances, tightly combined with neighbouring muscle tissues. There were no apparent connective tissues wrapped around the implants (Fig. 5a and b). At 12 weeks post-surgery, the composite implants of *g*-HAP/PLGA and HAP/PLGA became smaller appreciably, and the implants of pure PLGA were slender and fractured into several pieces because of degradation (Fig. 5c). At 20 weeks post-surgery, there were nearly no scaffolds left in the areas of the pure PLGA implants. However, in both *g*-HAP/PLGA and HAP/PLGA groups, one of the three implants was mineralized partly or completely, and the others disappeared mostly due to biodegradation. The mineralized implants became tough and were difficult to be separated from the neighbouring tissues (Fig. 5d).

*3.2.2. X-ray examination*

The intramuscular implants of *g*-HAP/PLGA, HAP/PLGA and PLGA were examined by CR at 4, 8, 12 and 20 weeks post-surgery. Fig. 6 shows the radiographs of the three parallel implants of each material at different time intervals. At 4, 8 and 12 weeks post-surgery, the implants of *g*-HAP/PLGA and HAP/PLGA can be seen clearly and kept their original shapes pretty nearly. There is no obvious mineralization shown in these implants. At 20 weeks post-surgery, only one of the three implants of *g*-HAP/PLGA or HAP/PLGA exhibits distinct mineralization, and the others lost their original shapes and became faint due to degradation. However, in the group of PLGA, the shapes of the implants changed slightly at 8 weeks

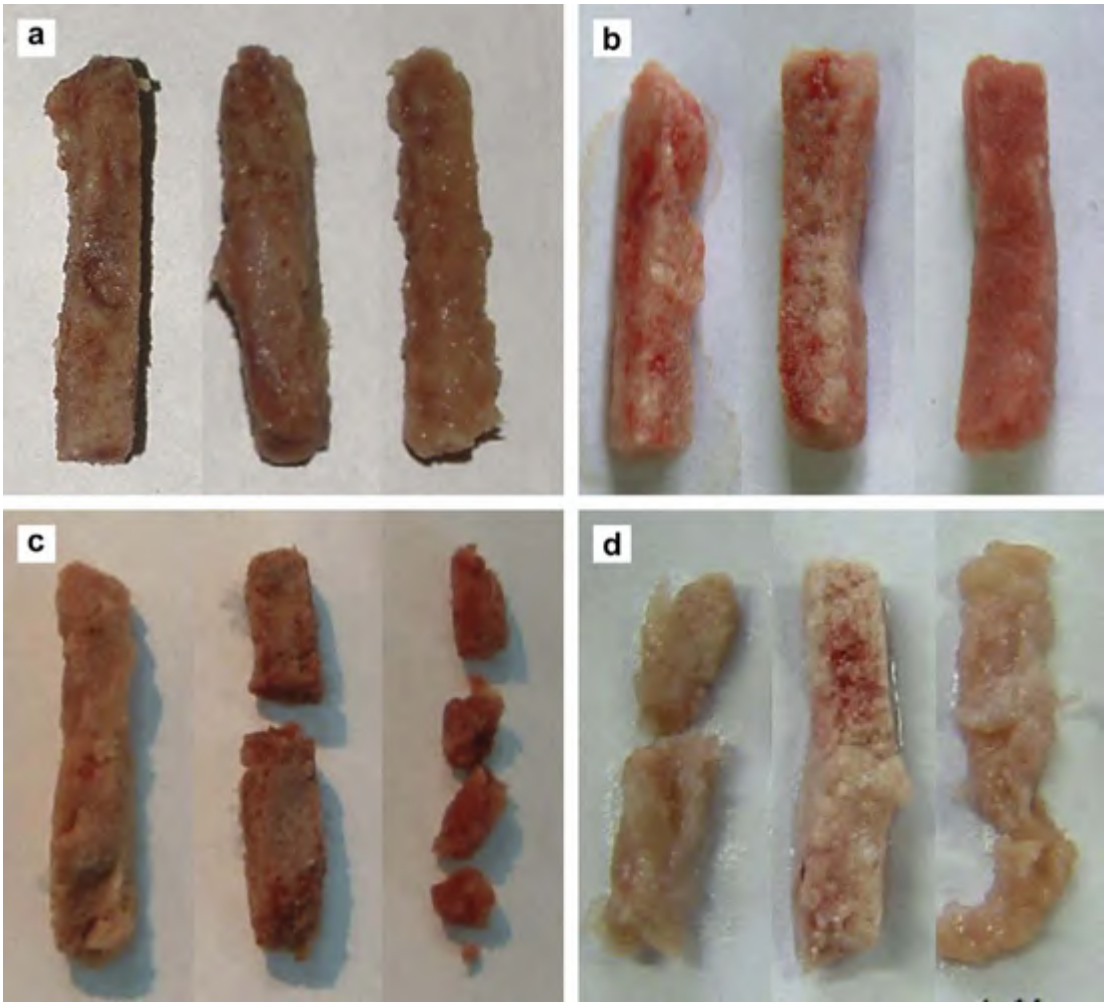


**Fig. 5.** Macroscopic observation of the representative implants of *g*-HAP/PLGA (left), HAP/PLGA (middle) and PLGA (right) scaffolds embedded in rabbit dorsal muscles at 4 (a), 8 (b), 12 (c) and 20 (d) weeks post-surgery. The photos were taken by Fujifilm FinePix S602 Digital Camera with 6× Optical Zoom.

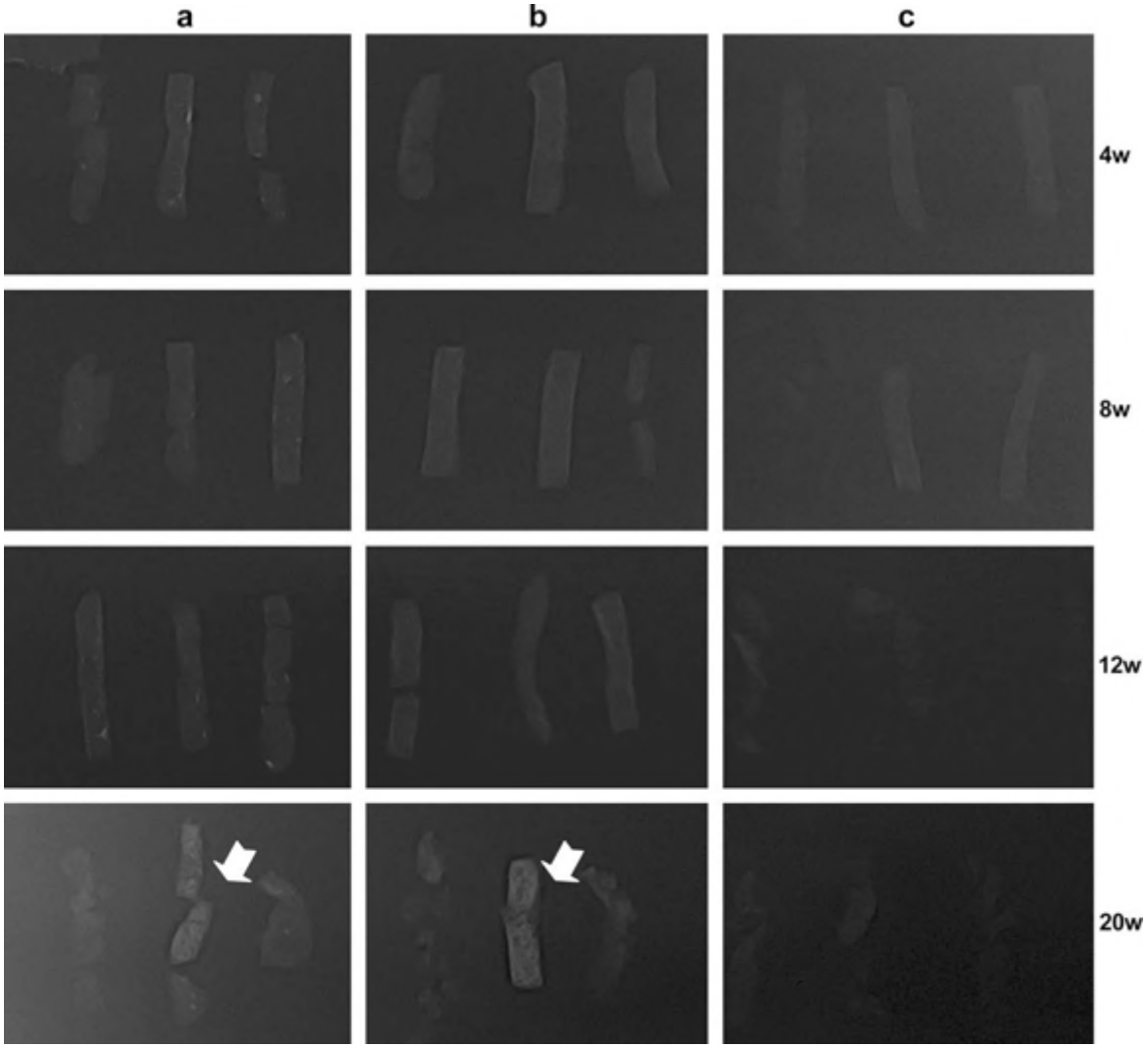


**Fig. 6.** Computer radiographs showing the mineralization and osteogenesis of the intramuscular implants of *g*-HAP/PLGA (a), HAP/PLGA (b) and PLGA (c) at 4, 8, 12 and 20 weeks post-surgery. At 20 weeks post-surgery, osteogenesis was observed distinctly in one of the three implants in both *g*-HAP/PLGA and HAP/PLGA groups, pointed by the arrow.

post-surgery and obviously at 12 weeks post-surgery. The radiographs of one implant at 8 weeks post-surgery and all three implants at 12 and 20 weeks post-surgery became faintness greatly. It indicated that the *g*-HAP or HAP filler could improve the stability of PLGA porous scaffold and prolong its biodegradation time. Meanwhile, the nanocomposite of PLLA grafted HAP as filler in PLGA matrix has the similar abilities to enhance *in vivo* mineralization and absorption as that of un-grafted HAP.

### 3.2.3. SEM analysis

Fig. 7 shows SEM photographs of the intramuscular implants of *g*-HAP/PLGA, HAP/PLGA and PLGA at 8 weeks post-surgery. The interfaces between the implant and the muscle tissue could be seen clearly in all three materials (Fig. 7a, c and e). The composite scaffolds of both *g*-HAP/PLGA and HAP/PLGA showed more loosen microstructure than PLGA, but there were more pores in *g*-HAP/PLGA than in HAP/PLGA to keep their original shapes. Compared to the composite scaffolds, the pores in PLGA disappeared due to biodegradation and replaced with the newly formed tissue. The results indicated that the surface modification of HAP with PLLA could improve the microstructure stability of the composite scaffold *in vivo*.

Moreover, at 8 weeks post-surgery, more mineral deposition and larger mineralized areas were observed in the composite scaffolds of *g*-HAP/PLGA and HAP/PLGA than that in the pure PLGA scaffold (Figs. 7 and 8). Fig. 8 shows typical mineralized and osteogenic areas in the implants of *g*-HAP/PLGA and HAP/PLGA at 8 weeks post-surgery with SEM and EDX analyses. It was honeycomb-like structure with a few of macro-pores ($>5$ μm) and an abundance of micro-pores ($<1$ μm) (Fig. 8a and b). EDX element analysis showed that the levels of Ca and P in these areas (Fig. 8c1) were significantly higher than those in other areas (Fig. 8c2) in the implants of *g*-HAP/PLGA and the pre-surgery scaffold of *g*-HAP/PLGA (Fig. 4a). The typical structures were found in the composite scaffolds of *g*-HAP/PLGA (Fig. 7b) and HAP/PLGA (Fig. 7d), but not in the implants of PLGA (Fig. 7f). It is concluded that the composite scaffolds of *g*-HAP/PLGA and HAP/PLGA exhibited similar ability of mineralization and both of them are better than the pure PLGA scaffolds.

### 3.2.4. ICP-AES analysis for calcium content measurement

Calcium contents in the intramuscular implants of *g*-HAP/PLGA, HAP/PLGA, and PLGA scaffolds at 4–20 weeks post-surgery were determined with ICP-AES (Fig. 9). The results show that the calcium contents of pre-surgery implants of *g*-HAP/PLGA and HAP/PLGA are $2.94 \pm 0.72$ wt% and $3.32 \pm 0.45$ wt%, respectively. Although the nanocomposites employed in this study is 10 wt% nano-particles of *g*-HAP or HAP in PLGA matrices, the difference of calcium contents

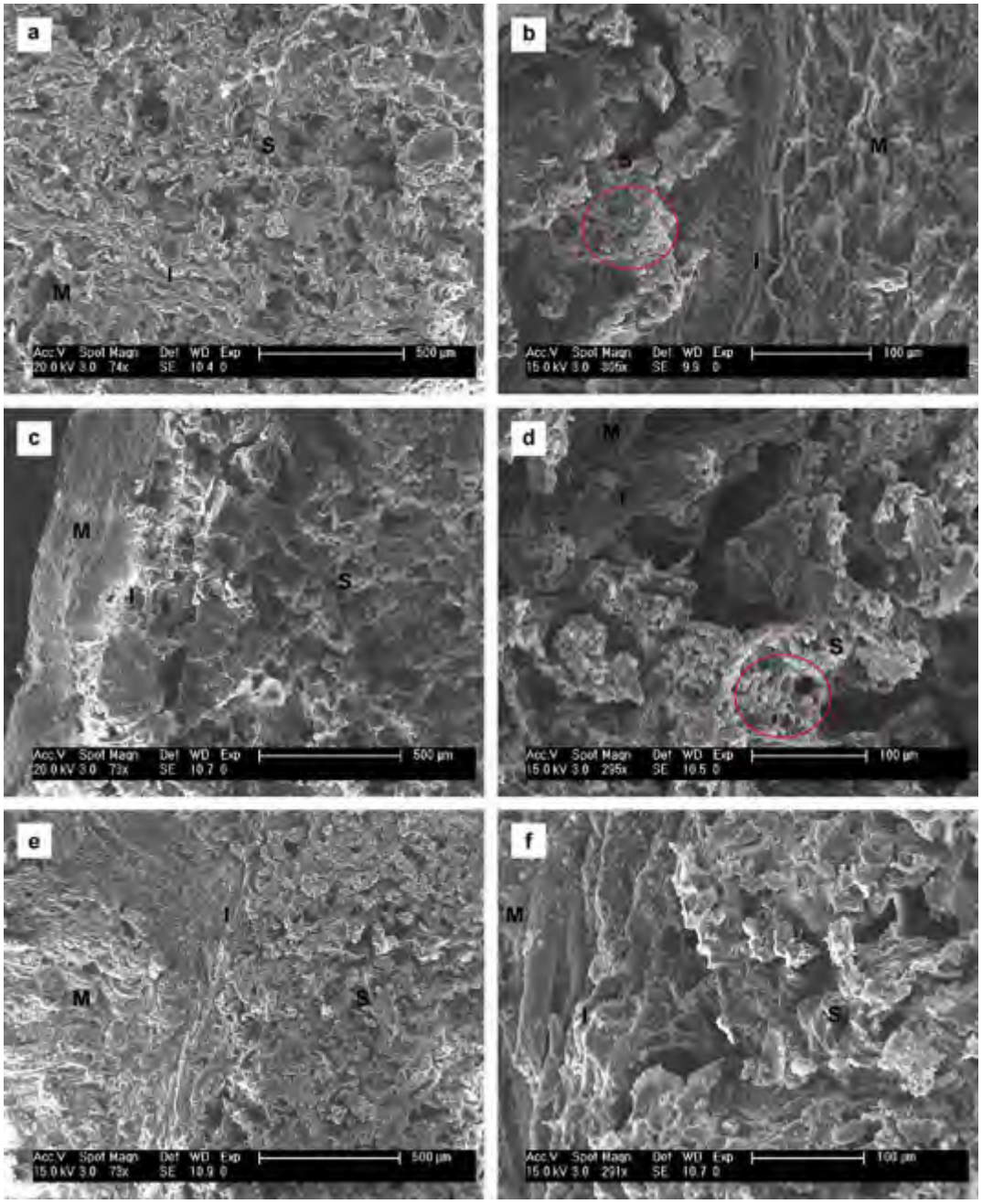


**Fig. 7.** SEM micrographs of the porous scaffolds of *g*-HAP/PLGA (a and b), HAP/PLGA (c and d), and PLGA (e and f) embedded in rabbit back muscle for 8 weeks. *S* is the area of scaffold implant, *M* is the area of muscle tissue, and *I* is the interface between the implant and the muscle tissue. The red circles in (b) and (d) represent the typical mineralized areas in the implants of *g*-HAP/PLGA and HAP/PLGA, respectively. Bar lengths are 500 μm (a, c and e) and 100 μm (b, d and f). [For interpretation of the references to color in this figure legend, the reader is referred to the web version of this article.]

between *g*-HAP/PLGA and HAP/PLGA is resulted from 5.0–6.0 wt% grafting PLLA in *g*-HAP particles. During 4–12 weeks post-surgery, calcium contents in both *g*-HAP/PLGA and HAP/PLGA groups were kept nearly at the same levels as pre-surgery. Only in HAP/PLGA group, there is a slight increase in calcium content at 8 weeks post-surgery compared to that of pre-surgery, and the level of calcium content is $4.16 \pm 0.02\%$.

At the 20 weeks post-surgery, calcium contents in one of the three implants in both *g*-HAP/PLGA and HAP/PLGA groups go steeply up to 18.7 wt% and 19 wt%, respectively, nearly 6 times more than that of pre-surgery. The others are 2.09 wt% and 2.26 wt% in *g*-HAP/PLGA group, and 5.82 wt% and 4.53 wt% in HAP/PLGA group. In contrast, the calcium contents in PLGA group are kept at a lower level of 0–0.29 wt% at all time intervals. It indicates that the composite scaffolds containing *g*-HAP or HAP nanoparticles have two possible outcomes, complete degradation or committed osteogenesis, which depend on the neighbouring micro-environment of an implant, such as osteogenetic cells, growth factors, enzymes and pH value, etc. The obtained ICP results are in good agreement with the radiographs of X-ray examination.

### *3.2.5. Histological analysis*

The histological analysis of the intramuscular implants of *g*-HAP/PLGA, HAP/PLGA and PLGA at 8 weeks post-surgery was undertaken with H&E staining and Masson's trichrome staining

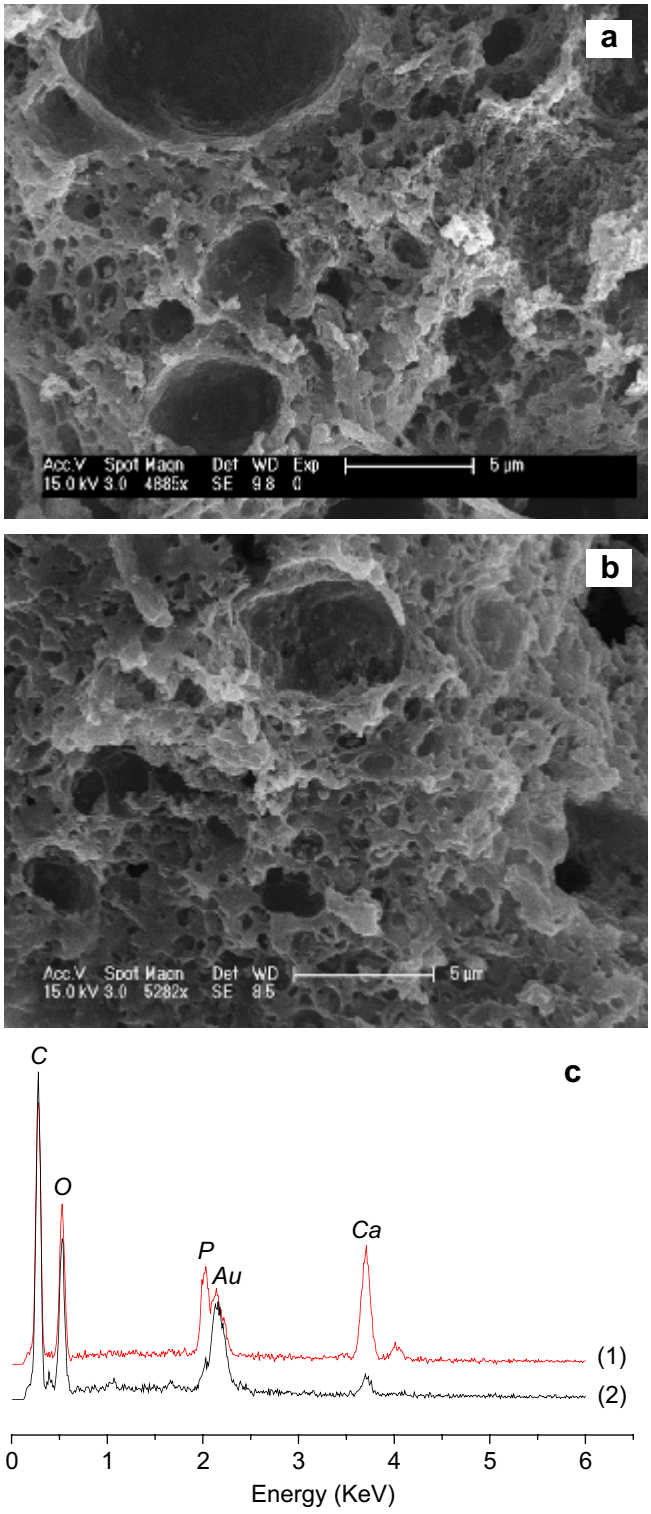


**Fig. 8.** SEM and EDX analysis of the intramuscular implants of *g*-HAP/PLGA and HAP/PLGA at 8 weeks post-surgery. (a) and (b) Amplificatory SEM micrographs of the circled areas in Fig. 7b and d, which showed the typical mineralized and osteogenic areas with a few of macro-pores (>5 μm) and an abundance of micro-pores (<1 μm) in the implants of *g*-HAP/PLGA (a) and HAP/PLGA (b), respectively. (c) High levels of Ca and P in these mineralized areas (c1) compared to the other areas (c2) in the implant of *g*-HAP/PLGA with EDX analysis. Bar lengths of (a) and (b) are 5 μm.

(Figs. 10 and 11). Fig. 10 shows the H&E staining of the three implants. Left pictures show the interfaces between the implants and the muscle tissues (a-1, b-1 and c-1) and the right ones show the central areas of the implants (a-2, b-2 and c-2).

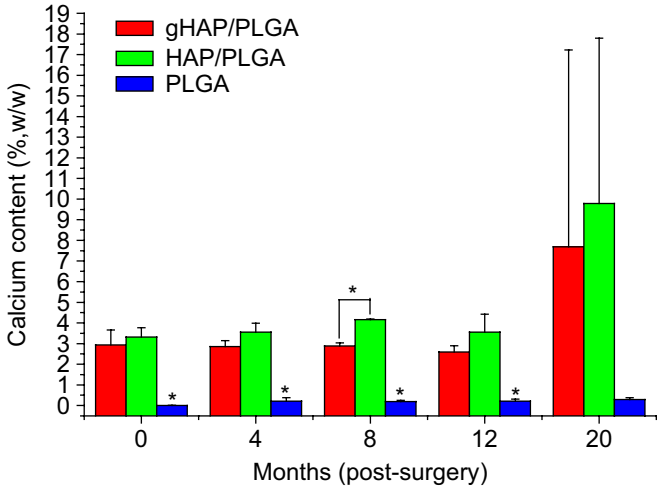


**Fig. 9.** ICP-AES analysis showing calcium contents of the intramuscular implants of *g*-HAP/PLGA, HAP/PLGA and PLGA porous scaffolds embedded in rabbit dorsal muscles at 0 (pre-surgery), 4, 8, 12 and 20 weeks post-surgery. Large standard deviations in *g*-HAP/PLGA and HAP/PLGA at 20 weeks post-surgery resulted from only one of three implants for each composite mineralized highly.

The pore structure of the scaffolds can be seen clearly in all implants of *g*-HAP/PLGA, HAP/PLGA and PLGA at 8 weeks post-surgery. There are a lot of multinucleate giant cells at both the edge area and the center area in *g*-HAP/PLGA. The cells with dense round nucleus and nucleolus, assembled together in the pore like an island or a strip around the pore wall (Figs. 10a and b and 11b and c). The similar multinucleate giant cells are found in HAP/PLGA, but the cells necrosed mostly. Some nuclei are irregular and faint, and the others disappeared and remained hollow. There are no multinucleate giant cells observed in PLGA implant. Meanwhile, Masson's trichrome staining shows that there are more collagen fibers (dark green) formed in *g*-HAP/PLGA than in other two materials (Fig. 11).

### 3.3. Implants in radius defects

Bone repair experiments were carried out using critically sized 2.0 cm radius defects replaced with cell-free material bars. Only one animal died from excessive anesthetization, and the others survived surgery. There were no significant post-operative events or adverse reactions to the treatment. The animals were examined with the CR radiographs at different time intervals and sacrificed for histological analysis at 8 weeks post-surgery.

#### 3.3.1. X-ray examination

Fig. 12 depicts typical radiographic results of rabbit radius defects (2.0 cm in length) repaired with the implant of BMP-2/*g*-HAP/PLGA, *g*-HAP/PLGA, HAP/PLGA and PLGA at 0, 2, 4, 8 weeks post-surgery. At the beginning (the first day after surgery), no obvious images were observed at the bone defect areas in all groups.

At 2 weeks post-surgery, bone formation at the defect areas results in various degrees of bridging between the two ends of the neighbouring bones in all groups. The radiographs at the repaired areas of BMP-2/*g*-HAP/PLGA, *g*-HAP/PLGA and HAP/PLGA groups appear similar and the implants exhibited distinct mineralization (Fig. 12a-2, b-2 and c-2). Except for the group of *g*-HAP/PLGA, in which an accidental ulna fracture forced the implant to move abnormally, the implants in the groups of BMP-2/*g*-HAP/PLGA and HAP/PLGA have been conjugated tightly with the ends of neighbouring bones. Compared to the others, there is more quantity of new bone formation in the group of BMP-2/*g*-HAP/PLGA. In

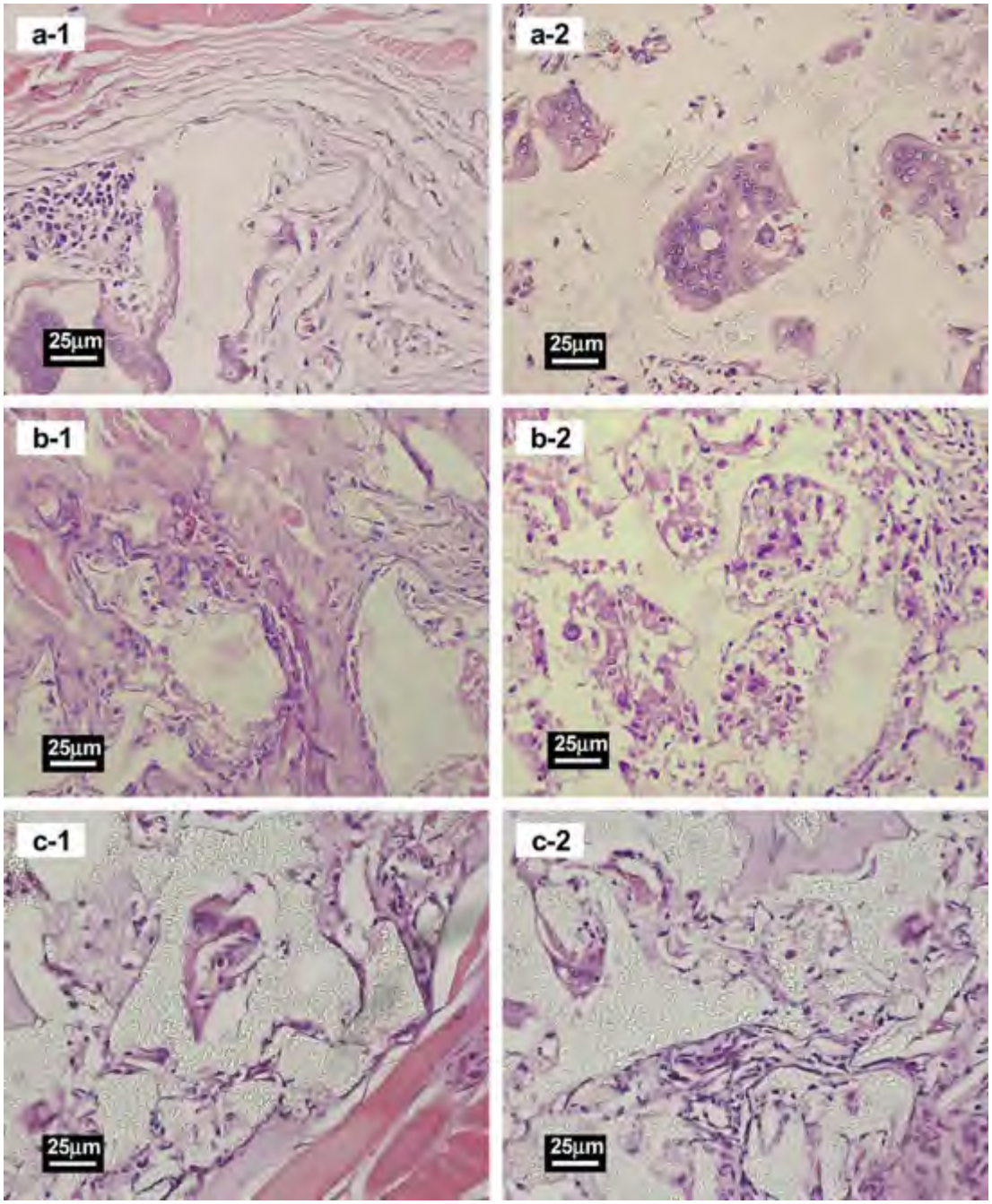


**Fig. 10.** Histological analysis showing the representative micrographs of *g*-HAP/PLGA (a-1 and a-2), HAP/PLGA (b-1 and b-2) and PLGA (c-1 and c-2) implanted intramuscularly for 2 months. Left pictures (a-1, b-1, c-1) show the adjacent area of the implants to the muscles, and right pictures (a-2, b-2 and c-2) show the center area of the implants. H&E staining. All scale bars are 25 μm.

contrast, in the group of PLGA, only the surface and the end areas of the implant near to the neighbouring bone tissues show gentle mineralization (Fig. 12d-2).

At 4 and 8 weeks post-surgery, the densities of the repaired areas in all groups increased gradually (Fig. 12). The bone bridges were more perfect and smooth in the groups of BMP-2/*g*-HAP/PLGA and HAP/PLGA (Fig. 12a-3,4 and c-3,4). In the group of *g*-HAP/PLGA, the previous gap between the implant and the neighbouring bone was shortened obviously at 4 weeks post-surgery (Fig. 12b-3) and disappeared at 8 weeks post-surgery (Fig. 12b-4). There is still a large area of bone defect, nearly half of the original defect, remained in the group of PLGA at 8 weeks post-surgery although the bone formation was guided on the surface of the implant from periosteum and resulted in a slender bridging (Fig. 12d-3,4).

The results indicated that the composite of PLGA with *g*-HAP or HAP allows more rapid mineralization, conjugation with neighbouring bone and osteogenesis than pure polymer scaffold. The incorporation of BMP-2 could improve the mineralization and osteogenesis of *g*-HAP/PLGA, and speed the bone healing process. Without HAP component, the polymer scaffold elicits bone formation mainly from the periosteum of the nearby radius.

### 3.3.2. Histological analysis

The photomicrographs of cross-sections through the radius bone defect sites implanted with BMP-2/*g*-HAP/PLGA, *g*-HAP/PLGA

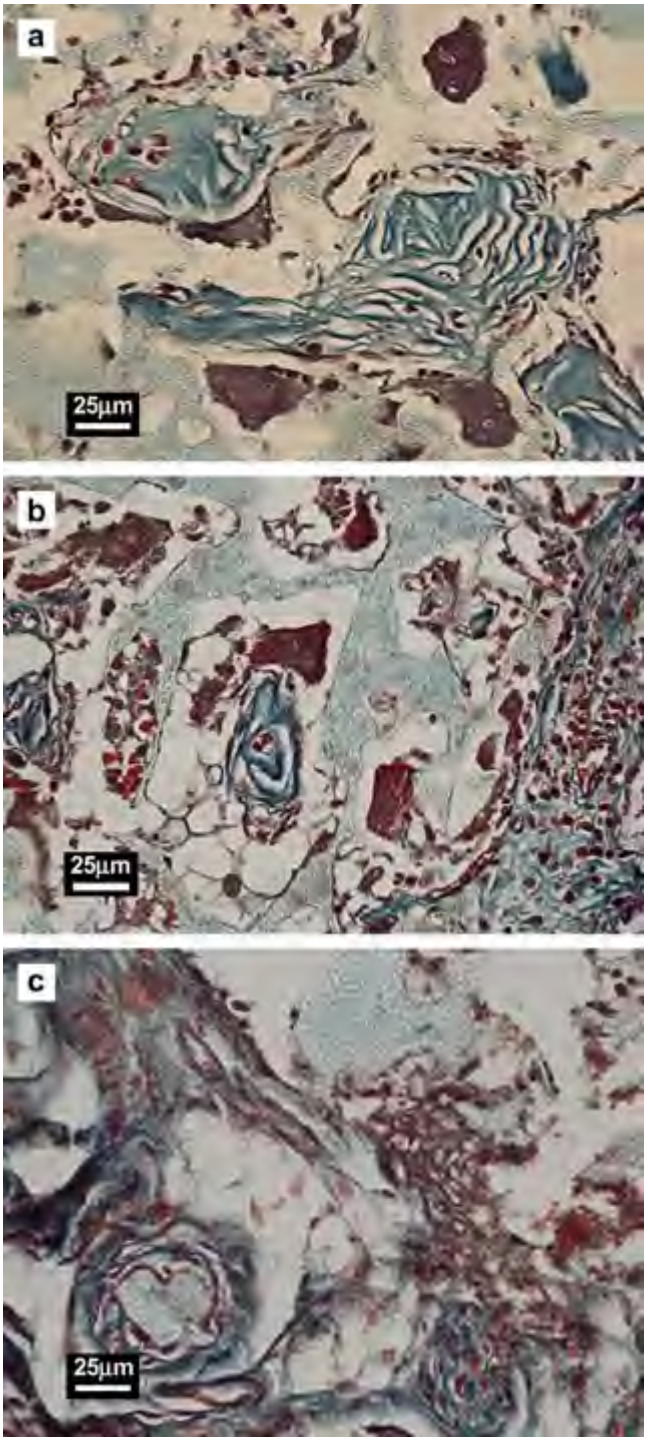


**Fig. 11.** Masson's trichrome staining showing the micrographs of the *g*-HAP/PLGA (a and b), HAP/PLGA (c and d) and PLGA (e and f) implants embedded in rabbit dorsal muscles. Red color shows muscle tissue, dark green color shows collagen fiber, and red yellow shows blood cells. Scale bars are 25 μm (a, c and e) and 250 μm (b, d and f). [For interpretation of the references to color in this figure legend, the reader is referred to the web version of this article.]

HAP/PLGA and PLGA scaffolds at 8 weeks post-surgery are presented in Fig. 13. The defect sites implanted with either BMP-2/*g*-HAP/PLGA, *g*-HAP/PLGA or HAP had the similar histological appearances (Fig. 13a–c). In these groups, the newly formed bones possess intact structures of a long bone, including a tubular bone stem with continuous thick cortex and a marrow cavity filled with bone marrow in the center of the stem. The bone stem in the group of BMP-2/*g*-HAP/PLGA was larger than those in *g*-HAP/PLGA and HAP/PLGA. Unabsorbed scaffolds were located in a triangle area near the ulna and the new bone of radius in these groups. In contrast, in the group of PLGA implant, only a layer of irregular thin cortex covered on the surface of the scaffold and no marrow cavity formed in the new bone was observed (Fig. 13d).

The interfaces between the new bones and the scaffolds are shown in Fig. 14. In the groups of BMP-2/*g*-HAP/PLGA and *g*-HAP/PLGA, the interfaces were regular and a layer of obvious fibrillar connective tissue was formed in the interface (Fig. 14a and b). However, the interfaces are irregular and there were no obvious fibrillar connective tissues in the groups of HAP/PLGA and PLGA (Fig. 14c and d). In the areas of residual scaffolds, there was a large quantity of multinucleate giant cells in all groups. The cells appeared in the pores of scaffolds and were near to the surface of the pore walls. It indicated that the multinucleate giant cells played an important role in scaffold degradation and osteogenesis like osteoclasts or osteoblasts.

## 4. Discussion

Tissue engineering provides a new approach for the therapy of damaged tissue or organ failure. The development of bone tissue engineering is directly related to changes in materials technology, especially the development of biomaterials that can be used in the reconstruction of large orthopaedic defects and are mechanically more suitable to their biological environment [2]. According to our previous work, the nanocomposite of *g*-HAP/PLLA and *g*-HAP/PLGA exhibited a series of prospective features, including better biocompatibility, enhanced mechanical property and improved thermal stability [19–21]. Human chondrocytes and rabbit osteoblasts could attach, spread and grow well on the surface of the nanocomposites. In order to be used as the orthopaedical substitutes, in this paper, we prepared a 3-D structural scaffold of *g*-HAP/PLGA, which is the PLGA matrix containing 10% (w/w) hydroxyapatite nano-particles surface-grafted with PLLA (*g*-HAP). The *in vivo* mineralization and osteogenesis of *g*-HAP/PLGA were studied through the intramuscular implants and the implants for repairing critical bone defects.

Synthesized scaffolds for osteogenesis should mimic bone morphology, structure and function to optimize integration into surrounding tissue. It is well-known that bone is a structure composed of hydroxyapatite ($Ca_{10}(PO_4)_6(OH)_2$) crystals deposited within an organic matrix (95% is type I collagen) [23]. Hydroxyapatite synthesized in nanometric-scale seems more similar to bone apatite, and it has the ability to promote the attachment of cultured osteoblasts and to improve their metabolic activity [1,24,25]. Addition of artificial hydroxyapatite had been approved to increase mineralization in matrices *in vitro* osteoblasts culture [26]. The particles provide anchorage for osteoblastic cells and provide a more favourable surface for cell attachment, determine the ability of the material to support bone ingrowth or act as a biological template [27]. As one of apatite–organic polymer composites, *g*-HAP/PLGA we prepared mimics the component of natural bones that 10 wt% nano-particles of modified HA distributed in PLGA matrix uniformly. The polymer, PLGA in scaffold, is functioned as collagen matrix in the bone, providing the structural support for osteogenesis. The results showed that the porous scaffold of *g*-HAP/PLGA exhibited better biocompatibility as a substrate for cell growth and migration *in vivo* whenever it was as an intramuscular implant or replacement for bone defect.

Surface topography is important for cell attachment [27]. Pore wall roughness plays an important role in osteogenic outcomes as well as macroporosity (pore size >50 μm) [5]. It is regarded that surface roughness enhances attachment, proliferation and differentiation of anchorage-dependent bone forming cells [28]. The

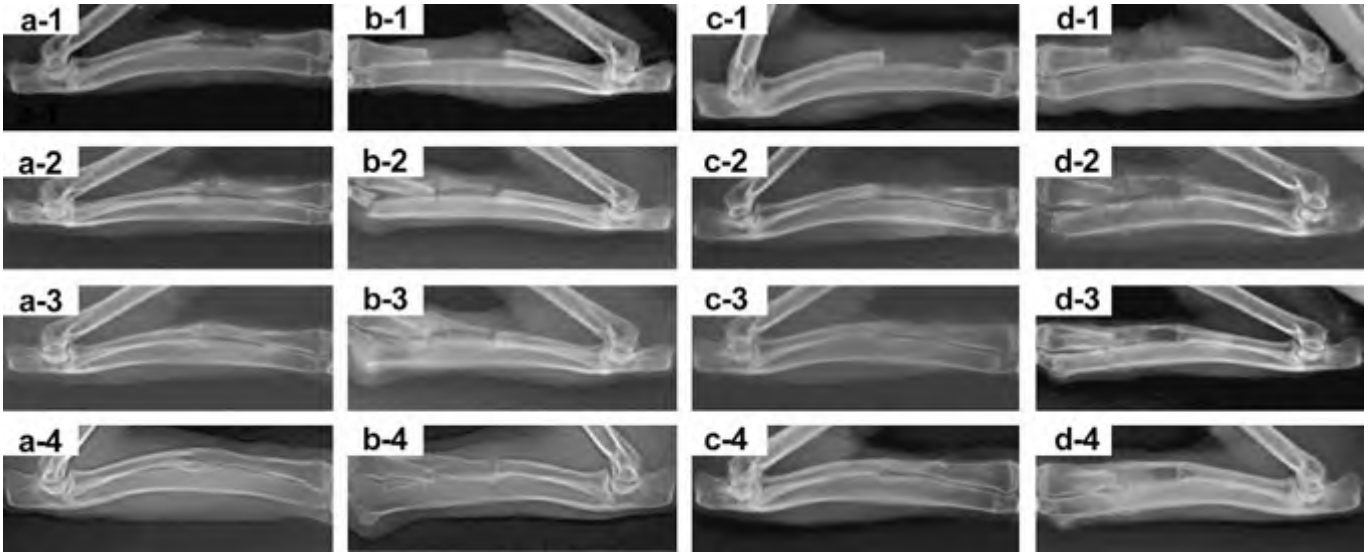


**Fig. 12.** Representative computer radiographs (CR) of rabbit radius defects implanted with the porous scaffolds of BMP-2/*g*-HAP/PLGA (a-1–4), *g*-HAP/PLGA (b-1–4), HAP/PLGA (c-1–4), and PLGA (d-1–4) at 0, 2, 4 and 8 weeks post-surgery. There were more mineral deposit and new bone formation in the groups of BMP-2/*g*-HAP/PLGA, *g*-HAP/PLGA, HAP/PLGA than that in the group of PLGA. (a-1, b-1, c-1 and d-1) 0 weeks (the first day after surgery); (a-2, b-2,c-2 and d-2) at 2 weeks; (a-3, b-3, c-3, and d-3) at 4 weeks; (a-4, b-4, c-4 and d-5) at 8 weeks.

surface energy may play a role in attracting particular proteins to the surface of the material and, in turn, this will affect the affinity of the cells to the material [2]. The composite scaffold of HAP/PLGA has been reported and showed better osteogenesis [18]. To improve the distribution of HAP nano-particles and the mechanical property of the nanocomposites, *g*-HAP used in this paper was obtained by surface-grafting with PLLA according to our previous work [19]. Compared to PLGA, the porous scaffold of *g*-HAP/PLGA or HAP/PLGA exhibited rougher pore walls due to the particles attached or inlayed on the surface of the wall. Moreover, the grafted HAP in

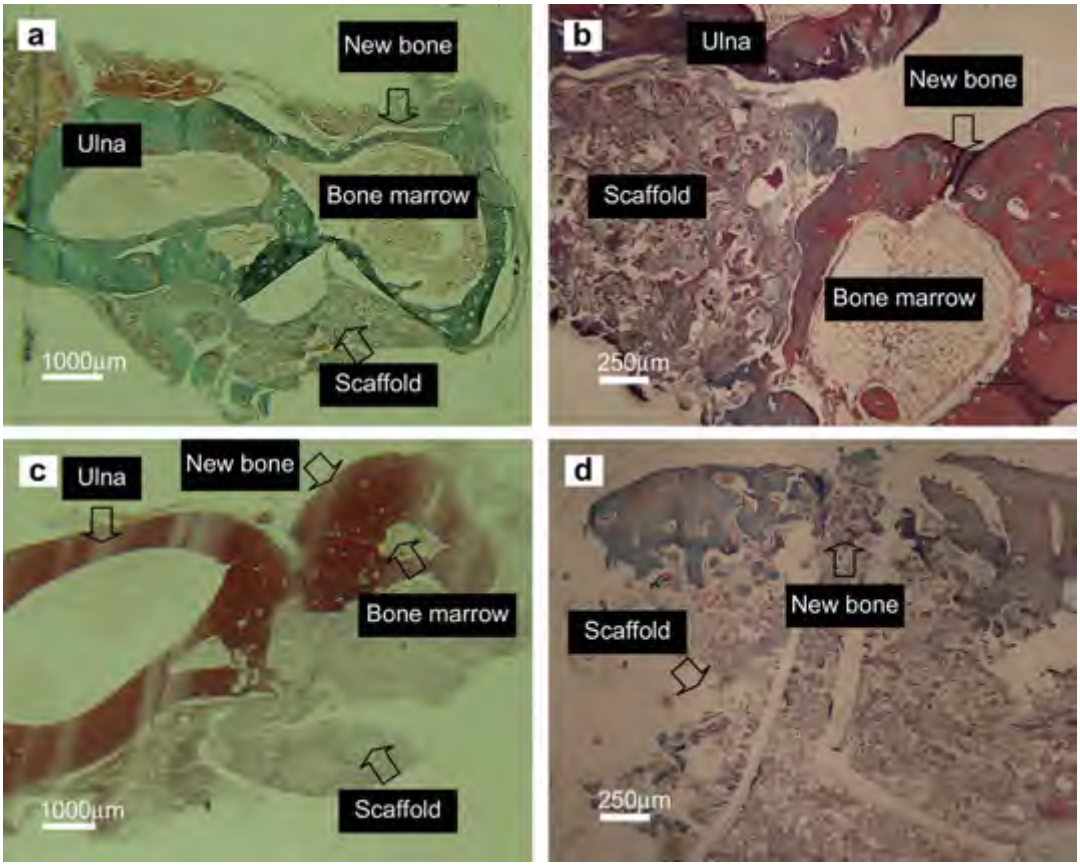


**Fig. 13.** Radius defects healing. Representative photomicrographs of cross-sections through the radius bone defect sites implanted with BMP-2/*g*-HAP/PLGA (a), *g*-HAP/PLGA (b), HAP/PLGA (c) and PLGA (d) scaffolds at 8 weeks post-surgery. The sections were treated with Masson's staining. (a and c) Taken by a digital camera and (b and d) taken by a light microscope. Scale bars are 1000 μm (a and c) and 250 μm (b and d).

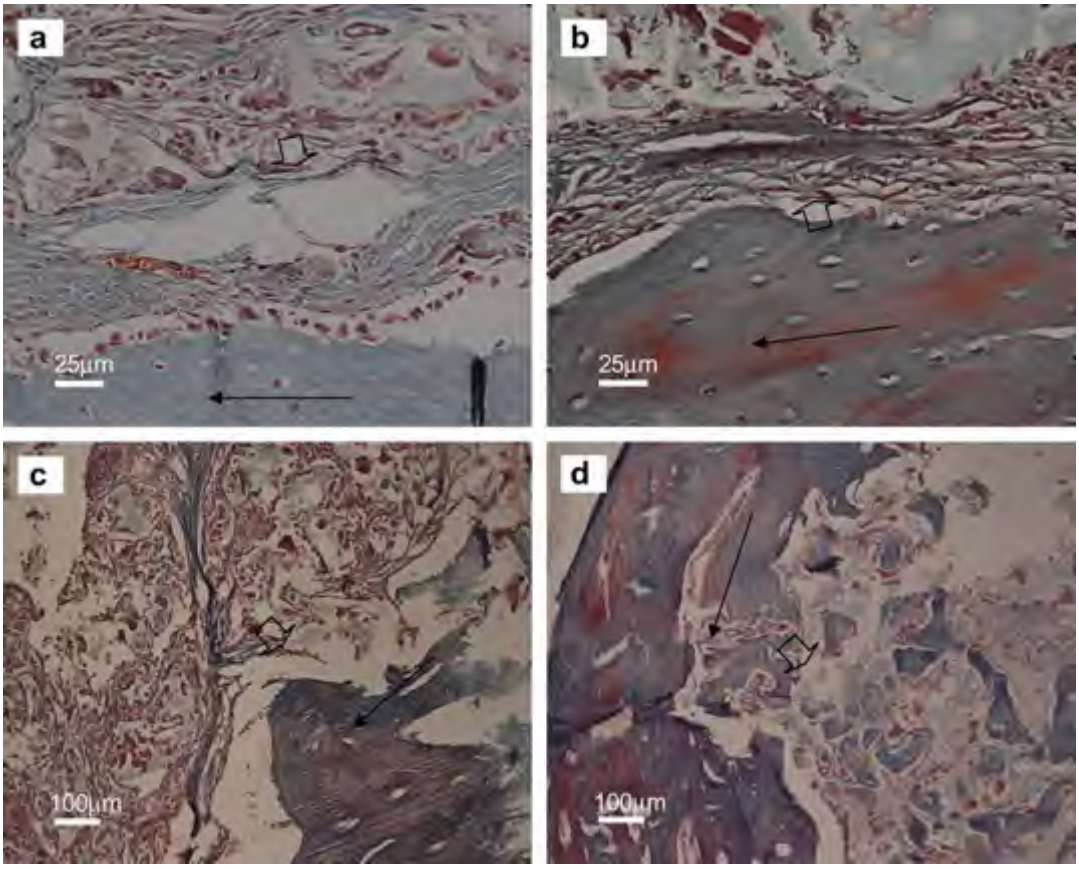


**Fig. 14.** Representative photomicrographs of vertical sections through the radius bone defect sites implanted with BMP-2/*g*-HAP/PLGA (a), *g*-HAP/PLGA (b), HAP/PLGA (c) and PLGA (d) scaffolds at 8 weeks post-surgery. The large arrows show the interfaces between the scaffolds and newly formed bones, and the slender arrows represent the axis orientations of the newly formed bones. Masson's trichrome staining. Scale bars are 25 μm (a and b) and 100 μm (c and d).

*g*-HAP/PLGA showed more uniform distribution on the wall than un-grafted HAP in HAP/PLGA.

At first, we worry about that the surface modification of HAP particles with PLLA will decrease their mineralization and osteogenesis. But results showed that the composite of *g*-HAP/PLGA has the similar mineralization and osteogenesis as HAP/PLGA although the actual content of HAP in *g*-HAP/PLGA was lower than that in HAP/PLGA. An interesting case was observed that one implant in the group of *g*-HAP/PLGA fractured and moved abnormally due to an accidental ulna fracture at 2 weeks post-surgery (Fig. 12b-2). Two weeks later, the fracture of the *g*-HAP/PLGA implant began to reach bone bonding (Fig. 12b-3) and disappeared completely at 8 weeks post-surgery (Fig. 12b-4). Meanwhile, the gap between the implant and the end of neighbouring bone due to implant moving was getting shorter and shorter (Fig. 12b2–4) and reached a bonding by the osteogenesis of *g*-HAP composite scaffold. A rapid developing process of bone repair was also observed in the group of BMP/*g*-HAP/PLGA which is similar to that of HAP/PLGA. At the defects repaired with pure PLGA, the initial mineralization began at the bilateral ends of the implant near to the neighbouring bone tissues, gradually reached toward the center of the implant from the two ends, and there was still a large no-mineral area remained in the center of the implant till 8 weeks post-surgery.

The processes of *in vivo* mineralization and biodegradation are complex for the porous nanocomposites scaffold of PLLA grafted and un-grafted nano-HAP in PLGA matrix. The balance among mineral deposition, biodegradation and tissue regeneration changed greatly at different time intervals of post-surgery. In this study, the scaffold of 10% *g*-HAP or HAP particles in PLGA matrix were used according to our previous study [20,21]. The intramuscular implant study showed that the composite scaffold of both *g*-HAP/PLGA and HAP/PLGA resulted in two possible outcomes, degradation completely or osteogenesis, in dorsal muscle at 5 months or 6 months post-surgery. It is also an interesting problem why only one or two but not all implants of *g*-HAP and HAP composite scaffolds turned to osteogenesis and the others degraded completely. Some unknown factors seem to impact on the balance as above-mentioned, such as the number of osteogenic cells, microvasculars, and osteoclasts (or multinucleate giant cells) in surrounding environment. Especially, multinucleate giant cells may play an important role in the final outcome of a synthesized implant.

In addition, the content of HAP in composite is also an important factor for mineralization and osteogenesis. It is regarded that increasing HA volume, enhances cellular response [27]. As a primary study in this paper, only 10% (w/w) of *g*-HAP in the composite of *g*-HAP/PLGA was used. As *g*-HAP is of hydroxyapatite grafted with PLLA, the actual content of HAP in *g*-HAP/PLGA is lower than HAP/PLGA. Compared to the group of HAP/PLGA, there were no obvious results of enhanced mineralization and osteogenesis in the group of *g*-HAP/PLGA observed in this study. We concluded that the main reason was the content of HAP (or the level of Ca and P) in *g*-HAP/PLGA being lower than that of HAP/PLGA. Therefore, in our following researches, the initial levels of Ca and P in materials should be designed to a comparative study for assessing the composites of hydroxyapatite and polymers as bone replacements.

## 5. Conclusion

A 3-D porous scaffold with the composite of PLGA and PLLA grafted nano-hydroxyapatite (*g*-HAP) has been prepared with the

solvent casting/particulate leaching method. The nano-particles of grafted HAP distributed on the surface of PLGA matrix more uniformly than that of un-grafted HAP. The intramuscular implant study showed that there were two outcomes for the nano-composite of *g*-HAP/PLGA, mineralized or biodegraded completely, which may be up to the content of HAP in polymer matrix and the balance of biodegradation, mineralization and tissue regeneration. As the bone replacement, the scaffold of *g*-HAP/PLGA exhibited rapid and strong osteoconductivity for repairing critical radius defects. The incorporation of BMP-2 could enhance the osteogenic process of the composite implant. It is concluded that the composite scaffold of *g*-HAP/PLGA exhibited the similar strong ability of mineralization, osteogenesis and biodegradation in intramuscular implants and replacement for bone defects although the levels of Ca and P exposure and the actual content of HAP in *g*-HAP/PLGA are lower than that in HAP/PLGA.

## Acknowledgements

This project is financially supported by the National Natural Science Foundation of China (no. 50673090), National Fund for Distinguished Young Scholar (no. 50425309) and the "863" Project (2007AA03Z320) from the Ministry of Science and Technology of China, as well as Major Project of International cooperation from the Ministry of Science and Technology of China (20071314).

## References

[1] Friedman CD, Costantino PD, Takagi S, Chow LC. BoneSource™ hydroxyapatite cement: a novel biomaterial for craniofacial skeletal tissue engineering and reconstruction. J Biomed Mater Res 1998;43:428–32.
[2] Burg KJL, Porter S, Kellam JF. Biomaterial developments for bone tissue engineering. Biomaterials 2000;21:2347–59.
[3] Coombes AG, Meikle MC. Resorbable synthetic polymers as replacements for bone graft. Clin Mater 1994;17:35–67.
[4] Laurencin CT, Attawia M, Borden MD. Advancements in tissue engineered bone substitutes. Curr Opin Orthop 1999;10:445–51.
[5] Karageorgiou V, Kaplan D. Porosity of 3D biomaterial scaffolds and osteogenesis. Biomaterials 2005;26:5474–91.
[6] Gunatillake PA, Adhikari R. Biodegradable synthetic polymers for tissue engineering. Eur Cell Mater 2003;5:1–16.
[7] Cleries L, Fernandez Pradas JM, Morenza JL. Behavior in simulated body fluid of calcium phosphate coatings obtained by laser ablation. Biomaterials 2000;2:1861–5.
[8] Klein CP, Driessen AA, de Groot K, van den Hooff A. Biodegradation behavior of various calcium phosphate materials in bone tissue. J Biomed Mater Res 1983;17:769–84.
[9] Nelson JF, Stanford HG, Cutright DE. Evaluation and comparison of biodegradable substances as osteogenic agents. Oral Surg 1977;43:836–43.
[10] Hollinger JO. Preliminary report on osteogenic potential of a biodegradable copolymer of polylactide (PLA) and polyglycolide (PGA). J Biomed Mater Res 1983;17:71–82.
[11] Wei J, Li YB. Tissue engineering scaffold material of nano-apatite crystals and polyamide composite. Eur Polym J 2004;3:509–15.
[12] Jung Y, Kim SS, Kim YH, Kim SH, Kim BS, Kim S, et al. A poly(lactic acid)–calcium metaphosphate composite for bone tissue engineering. Biomaterials 2005;26:6314–22.
[13] Rizzi SC, Heath DJ, Coombes AG, Bock N, Textor M, Downes S. Biodegradable polymer/hydroxyapatite composites: surface analysis and initial attachment of osteoblasts. J Biomed Mater Res 2001;55:475–86.
[14] Wei G, Ma P. Structure and properties of nano-hydroxyapatite-polymer composite scaffolds for bone tissue engineering. Biomaterials 2004;25:4749–57.
[15] Du C, Cui FZ, Zhu XD, de Groot K. Three-dimensional nano-HAp/collagen matrix loading with osteogenic cells in organ culture. J Biomed Mater Res 1999;44:407–15.
[16] Du C, Cui FZ, Feng QL, Zhu XD, de Groot K. Tissue response to nano-hydroxyapatite/collagen composite implants in marrow cavity. J Biomed Mater Res 1998;42:540–8.
[17] Stayton PS, Drobny GP, Shaw WJ, Long JR, Gilbert M. Molecular recognition at the protein-hydroxyapatite interface. Crit Rev Oral Biol Med 2003;14:370–6.
[18] Kim SS, Park MS, Jeon O, Choi CY, Kim BS. Poly(lactide-*co*-glycolide)/hydroxyapatite composite scaffolds for bone tissue engineering. Biomaterials 2006;27:1399–409.
[19] Hong ZK, Qiu XY, Sun JR, Deng MX, Chen XS, Jing XB. Grafting polymerization of L-lactide on the surface of hydroxyapatite nano-crystals. Polymer 2004;45:6705–13.
[20] Hong ZK, Zhang PB, He CL, Qiu XY, Liu AX, Chen L, et al. Nano-composite of poly(L-lactide) and surface grafted hydroxyapatite: mechanical properties and biocompatibility. Biomaterials 2005;26:6296–304.
[21] Hong ZK, Zhang PB, Liu AX, Chen L, Chen XS, Jing XB. Composites of poly (lactide-*co*-glycolide) and the surface modified carbonated hydroxyapatite nanoparticles. J Biomed Mater Res A 2007;81:515–22.
[22] Zhang R, Ma PX. Poly(α-hydroxyl acids)/hydroxyapatite porous composites for bone-tissue engineering. I. Preparation and morphology. J Biomed Mater Res 1999;44:446–55.
[23] Marks Jr SC, Odgren PR. Structure and development of the skeleton. In: Bilezikian JP, Raisz LG, Rodan GA, editors. Principles of bone biology. 2nd ed. San Diego: Academic Press; 2002. p. 3–15.
[24] Huang J, Best S, Bonfield W, Brooks RA, Rushton N, Jayasinghe SN, et al. In vitro assessment of the biological response to nano-sized hydroxyapatite. J Mater Sci Mater Med 2004;15:441–5.
[25] Pezzatini S, Solito R, Morbidelli L, Lamponi S, Boanini E, Bigi A, et al. The effect of hydroxyapatite nanocrystals on microvascular endothelial cell viability and functions. J Biomed Mater Res A 2006;76:656–63.
[26] Zimmermann B, Wachte HC, Noppe C. Patterns of mineralization in vitro. Cell Tissue Res 1991;263:483–93.
[27] Ciapetti G, Ambrosio L, Savarino L, Granchi D, Cenni E, Baldini N, et al. Osteoblast growth and function in porous poly ε-caprolactone matrices for bone repair: a preliminary study. Biomaterials 2003;24:3815–24.
[28] Yuan H, Kurashina K, de Bruijn JD, Li Y, de Groot K, Zhang X. A preliminary study on osteoinduction of two. kinds of calcium phosphate ceramics. Biomaterials 1999;20:1799–806.